ApJ, submitted 11/17/2006
Preprint typeset using LaTeX style emulateapj v. 10/09/06

arXiv:astro-ph/0611571v1 17 Nov 2006

DYNAMICAL MODELS OF ELLIPTICAL GALAXIES IN $Z = 0.5$ CLUSTERS: I. DATA-MODEL COMPARISON AND EVOLUTION OF GALAXY ROTATION

Roeland P. van der Marel
Space Telescope Science Institute, 3700 San Martin Drive, Baltimore, MD 21218

Pieter G. van Dokkum
Department of Astronomy, Yale University, New Haven, CT 06520
ApJ, submitted 11/17/2006

ABSTRACT

We present spatially resolved stellar rotation velocity and velocity dispersion profiles form Keck/LRIS absorption-line spectra for 25 galaxies, mostly visually classified ellipticals, in three clusters at $z \approx 0.5$. We interpret the kinematical data and HST photometry using oblate axisymmetric two-integral $f(E, L_z)$ dynamical models based on the Jeans equations. This yields good fits, provided that the seeing and observational characteristics are carefully modeled. The fits yield for each galaxy the dynamical M/L and a measure of the galaxy rotation rate. Paper II addresses the implied M/L evolution. Here we study the rotation-rate evolution by comparison to a sample of local elliptical galaxies of similar present-day luminosity. The brightest galaxies in the sample all rotate too slowly to account for their flattening, as is also observed at $z = 0$. But the average rotation rate is higher at $z \approx 0.5$ than locally. This may be due to a higher fraction of misclassified S0 galaxies (although this effect is insufficient to explain the observed strong evolution of the cluster S0 fraction with redshift). Alternatively, dry mergers between early-type galaxies may have decreased the average rotation rate over time. It is unclear whether such mergers are numerous enough in clusters to explain the observed trend quantitatively. Disk-disk mergers may affect the comparison through the so-called "progenitor bias", but this cannot explain the direction of the observed rotation-rate evolution. Additional samples are needed to constrain possible environmental dependencies and cosmic variance in galaxy rotation rates. Either way, studies of the internal stellar dynamics of distant galaxies provide a valuable new approach for exploring galaxy evolution.

Subject headings: galaxies: clusters: individual (CL3C295, CL0016+16, CL1601+42) — galaxies: evolution — galaxies: formation — galaxies: kinematics and dynamics.

1. INTRODUCTION

Elliptical galaxies form an important component of the galaxy population in the universe. In fact, they constitute the bulk of the population both at the high-mass end of the galaxy distribution and at the highest environmental densities (i.e., in clusters). An understanding of the formation and evolution of elliptical galaxies is therefore crucial for any successful theory of hierarchical structure formation in a cosmological context.

The most direct way to constrain the evolution of elliptical galaxies is through observations of their photometric and dynamical properties at intermediate and high redshifts. Several of the most successful techniques to use such data have relied on the statistical properties of globally averaged or characteristic galaxy quantities. For example, the fundamental plane is a correlation between the effective radius $r_{\rm eff}$, the average surface brightness $I_{\rm eff}$ inside the effective radius, and the velocity dispersion σ. The evolution of the fundamental plane can be used to place constraints on the formation redshifts of elliptical galaxies (as reviewed in van Dokkum & van der Marel 2006, hereafter vDvdM06). Similarly, the color-magnitude relation is a correlation between the total magnitude and globally averaged color. Elliptical galaxies form a "red sequence" that can also be used to constrain the formation redshifts of elliptical galaxies (e.g., De Lucia et al. 2004; Mei et al. 2006).

The success and popularity of studies based entirely on globally averaged or characteristic galaxy properties can be attributed at least in part to the relative ease with which such studies can be performed. In particular, no modeling or understanding of the internal structure of the sample galaxies is necessarily required. However, this is at the same time the main drawback of such studies. To draw conclusions one is usually forced to make some implicit assumptions about the structure of the galaxy, or at least, that this structure does not evolve with time. Such assumptions remain untested until one actually progresses to more detailed studies of the resolved galaxy structure. In fact, data that enable such studies are often available, but remain unused. For example, fundamental plane or color-magnitude relation studies do not use available information on the axial ratios of individual galaxies, their resolved surface brightness or color profiles, or any spatially resolved information on the kinematical structure of the galaxy.

One approach to learn more about the internal structure of distant elliptical galaxies is to construct detailed dynamical models for high-quality spatially resolved photometric and kinematic data. The required dynamical modeling tools exist, and high quality photometric data is available for many galaxies from the Hubble Space Telescope (HST). The most challenging part is therefore to obtain the necessary kinematic data. However, this is quite possible with large aperture telescopes equipped

with multi-slit spectrographs (e.g., Kelson et al. 2000). Treu & Koopmans (2004) and Koopmans et al. (2006) obtained and modeled resolved kinematical profiles for some lensing galaxies. They constructed relatively simple dynamical models (namely, parameterized spherical models) but this still allowed them to obtain several interesting new results on the dark halo component of these galaxies. There is no reason why similar methodologies or more detailed modeling approaches cannot be applied to other large samples of (non-lensing) early-type galaxies.

In vDvdM06 we presented spectroscopy with the Low Resolution Imager and Spectrograph (LRIS) on Keck of some two dozen galaxies in the intermediate-redshift ($z \approx 0.5$) clusters CL3C295, CL0016+16 and CL1601+42. The sample galaxies were selected to be bright enough for spectroscopy, and visually classified from the HST images of Dressler et al. (1997) and Smail et al. (1997) as early-type (and in most cases elliptical) galaxies. In vDvdM06 we only used the data for a study of the FP evolution of the three sample clusters. However, we obtained spectroscopic data that are deep enough to extract spatially resolved rotation curves and velocity dispersion profiles. Furthermore, in the multi-slit mask designs care was taken to tilt individual slits so that they were aligned preferentially with the major axes of the galaxies, insofar possible given geometric restrictions. We present the kinematical profiles here, and we construct detailed dynamical models to interpret them.

Our models are axisymmetric with two-integral distribution functions of the form $f = f(E, L_z)$. Here E is the energy and L_z the angular momentum around the symmetry axis. The internal dynamics are calculated by solving the Jeans equations of hydrostatic equilibrium. Models of this type have been constructed successfully for many nearby galaxies (e.g., Binney, Davies, & Illingworth 1990; van der Marel 1991; Magorrian et al. 1998; Corsini et al. 1999). Two-integral models are relatively simple in that they have $\overline{v_R^2} \equiv \overline{v_z^2}$. So they can be thought of as the axisymmetric generalization of spherical isotropic models. Of course, more sophisticated modeling approaches do exist (e.g., those that built completely general three-integral distribution functions using the technique of numerical orbit superposition; van der Marel et al. 1998; Gebhardt et al. 2003). However, the complexity of these models would be "overkill" as compared to the quality of the data that can be realistically obtained at intermediate redshifts.

The models yield the rotation rate of each galaxy by fitting to the spatially resolved kinematical profiles. The results can therefore be used to study the evolution of the rotation rate of galaxies as a function of time. This evolution can yield new insights into the mechanisms by which the internal structure of elliptical galaxies gets modified through mergers. Mergers are believed to be characteristic of the hierarchical build up of all structure in the Universe. However, the relative importance of different types of mergers remains poorly constrained. While the formation of elliptical galaxies through disk-disk mergers has received considerable attention historically (e.g., Barnes 1988), much recent work has focused on the importance of "dry" mergers between early-type galaxies (van Dokkum 2005; Bell et al. 2006). Such mergers produce remnants with different rotational properties. Disk-disk mergers tend to produce remnants with relatively rapid rotation (Naab & Burkert 2003; Naab, Jesseit & Burkert 2006b), whereas dry mergers tend to produce remnants with relatively little rotation (Naab, Khochfar & Burkert 2006a). A study of the evolution of galaxy rotation properties can therefore contribute to an improved understanding of the actual mechanisms that have shaped todays elliptical galaxies.

The inferred rotation rates of the sample galaxies also provide the potential to kinematically identify S0 galaxies that have been visually misclassified as elliptical galaxies. S0 galaxies make up only 12% to 21% of the galaxy population in the three clusters studied here, compared to 50% to 60% for nearby clusters (Dressler et al. 1997). In the three clusters, visually-classified elliptical galaxies outnumber S0 galaxies by a ratio of $\sim 3:1$, whereas in nearby clusters S0 galaxies outnumber elliptical galaxies. Issues of misclassification have been raised as a potential contributing factor to this strong apparent evolution of the S0 fraction (e.g., Fabricant et al. 2000). This may be relevant for CL3C295 and CL0016+16, given that their deficit of S0 galaxies is compensated by an overabundance of elliptical galaxies (which constitute more than 50% of the population). In these two clusters the total early-type galaxy fraction (i.e., elliptical and S0 galaxies combined) is only slightly lower than in nearby clusters. By contrast, in CL1601+42 the majority of galaxies are spirals, which outnumber the S0 galaxies by a factor of 4–5.

The layout of the present paper is as follows. Section 2 discusses the details of the modeling approach. Section 3 presents the results for the individual galaxies in the sample. Section 4 discusses the inferred rotation properties of the intermediate-redshift sample galaxies, compares them to the rotation properties of early-type galaxies in the local Universe, and discusses the results. Section 5 presents a summary and discussion of the paper's main conclusions.

The dynamical models also yield the mass-to-light ratios M/L for all the galaxies. These are used in van der Marel & van Dokkum (2006, hereafter Paper II) to study the M/L evolution of elliptical galaxies as a function of redshift. This complements and tests analyses based on Fundamental Plane evolution, such as those presented in vDvdM06.

Throughout both papers we assume a cosmology with $\Omega_{\rm m} = 0.27$, $\Omega_\Lambda = 0.73$ (the values obtained by the Wilkinson Microwave Anisotropy Probe; Spergel et al. 2003) and $H_0 = 71\,{\rm km\,s^{-1}\,Mpc^{-1}}$ (the value obtained by the HST Cepheid Key Project; Section 7 of Freedman et al. 2001).

2. DYNAMICAL MODELS

For the two-integral dynamical modeling we have used the assumptions and software described previously by van der Marel et al. (1994b). The goal is to first find a light density distribution that is consistent with observed HST photometry, and then to find a dynamical solution of the Jeans equations that reproduces the observed Keck spectroscopy. Fitting the model to the kinematics yields both a normalized measure k of the galaxy's rotation rate and the dynamical M/L over the spectroscopically explored region.

The three-dimensional mass density is assumed to be oblate axisymmetric and of the form

$$\rho(R,z) = \rho_0 (m/b)^\alpha [1+(m/b)^2]^\delta, \quad m^2 \equiv R^2 + z^2 Q^{-2}. \tag{1}$$

Here z is the symmetry axis of the galaxy and (R,ϕ,z) are the usual cylindrical coordinates. All isodensity surfaces are spheroids with axial ratio $Q \leq 1$. The adopted mass density has no particular physical significance. It is merely a convenient parameterization in which the parameters ρ_0, b, α and δ provide sufficient freedom to adequately fit the data available for the sample galaxies. The components of the force $\vec{\nabla}\Phi$ (where Φ is the gravitational potential) exerted by the matter with mass density given in equation (1) can be expressed as one-dimensional integrals (Binney & Tremaine 1987, eq. [2-88]) that are easily evaluated numerically.

The Jeans equations for hydrostatic equilibrium in a two-integral model

$$\begin{aligned} &\frac{\partial \rho \overline{v_z^2}}{\partial z} + \rho \frac{\partial \Phi}{\partial z} = 0, \\ &\frac{\partial \rho \overline{v_R^2}}{\partial R} + \rho \frac{\partial \Phi}{\partial R} + \frac{\rho}{R}\left[\overline{v_R^2} - \overline{v_\phi^2}\right] = 0, \end{aligned} \tag{2}$$

form a closed set for the two unknowns $\overline{v_\phi^2}$ and $\overline{v_R^2} \equiv \overline{v_z^2}$. For known ρ and $\vec{\nabla}\Phi$ the equations can be solved numerically on a two-dimensional grid in the meridional plane. The amount of mean streaming in the model is unconstrained by the condition of hydrostatic equilibrium. We therefore introduce a free parameter k that assigns an amount of rotational support according to

$$\overline{v_\phi} = k[\overline{v_\phi^2} - \overline{v_R^2}]^{1/2}. \tag{3}$$

For $k = 0$ the model is non-rotating, whereas for $|k| = 1$ the velocity dispersion tensor is isotropic and the model is a so-called "oblate isotropic rotator". The maximum value of $|k|$ for a physical model is defined by the criterion that $\sigma_\phi^2 \equiv \overline{v_\phi^2} - \overline{v_\phi}^2$ is everywhere positive. This implies that

$$|k| \leq k_{\max} = \min_{(R,z)} \left[\, \overline{v_\phi^2}/(\overline{v_\phi^2} - \overline{v_R^2}) \,\right]^{1/2}. \tag{4}$$

For line-of-sight projection we adopt a Cartesian coordinate system (x,y,w) with w along the line of sight, (x,y) in the plane of the sky, and x along the major axis. The projected mass density is

$$\Sigma(x,y) = \int_{-\infty}^{\infty} \rho(x,y,w)\, dw. \tag{5}$$

We assume that the mass-to-light ratio M/L (expressed throughout this paper in units of $\mathrm{M}_\odot/\,\mathrm{L}_\odot$) is constant with radius in the galaxy. This is known to be a reasonable assumption when modeling kinematical data inside the effective radius of elliptical galaxies (van der Marel 1991; Kronawitter et al. 2000). The projected light density is then $\mu(x,y) = \Sigma(x,y)/(M/L)$. When viewed at inclination angle i, the projected contours are similar ellipses with projected axial ratio Q', with

$$Q'^2 \equiv \cos^2 i + Q^2 \sin^2 i. \tag{6}$$

Two models of the same Q' and different inclination predict exactly the same projected light density if they have the same values of b, α, δ, and $j_0 Q$, where $j_0 \equiv \rho_0/(M/L)$ is a luminosity density.

The projected luminosity-weighted line-of-sight velocity moments of order i are given by

$$\langle \overline{v_w^i} \rangle (x,y) = \frac{1}{\Sigma(x,y)} \int_{-\infty}^{\infty} \rho(x,y,w)\, \overline{v_w^i}(x,y,w)\, dw. \tag{7}$$

In the present context we are interested only in the first two moments. For a two-integral system

$$\begin{aligned} \overline{v_w} &= \overline{v_\phi} \cos\phi \sin i, \\ \overline{v_w^2} &= (\overline{v_\phi^2} - \overline{v_R^2}) \cos^2\phi \sin^2 i + \overline{v_R^2}. \end{aligned} \tag{8}$$

The resulting line-of-sight integrals can be evaluated numerically once the Jeans equations have been solved.

The observational setup is characterized by the slit width W, the pixel scale P in the spatial direction, and the seeing FWHM S. The model predictions $\langle \overline{v_w^i} \rangle (x,y)$ must therefore be convolved (in an intensity-weighted sense) both with a square tophat function of size $W \times P$ and with the seeing point-spread function (PSF). The latter was assumed to be Gaussian. For the convolutions we used a Monte-Carlo integration procedure. This ultimately yields for each spatial pixel (or set of binned pixels) along the slit the model predictions for the mean velocity V and for the second velocity moment $\sigma_{\mathrm{RMS}}^2 \equiv V^2 + \sigma^2$, where σ is the velocity dispersion.

For a given inclination, the model parameters j_0, b, α, δ and Q can be fixed by fitting the projected light density $\mu(x,y)$ to the available galaxy imaging, which was calibrated to the rest-frame B-band. To transform the best-fitting luminosity density of each model to units of $\mathrm{L}_\odot\,\mathrm{pc}^{-3}$ we adopted a solar absolute B-band magnitude $M_{B,\odot} = 5.48$ (Binney & Merrifield 1998) and the relation between arcsec and pc dictated by the adopted redshift and cosmology. For the model thus obtained we solve the Jeans equations using the trial values $M/L = 1$ for the mass-to-light ratio and $k = 1$ for the rotational support. The results are projected along the line-of-sight and convolved with the observational setup. Let the predictions thus obtained be $\hat{V}$ and $\hat{\sigma}_{\mathrm{RMS}}$. The predictions for other values of M/L and k are then obtained by simple linear scaling: $\hat{V} \rightarrow k(M/L)^{1/2}\hat{V}$ and $\hat{\sigma}_{\mathrm{RMS}} \rightarrow (M/L)^{1/2}\hat{\sigma}_{\mathrm{RMS}}$. Let the observed mean velocity and velocity dispersion be V_{obs} and σ_{obs}. The data-model comparison residuals are then $\delta V = V_{\mathrm{obs}} - V_{\mathrm{sys}} - k\,(M/L)^{1/2}\,\hat{V}$ and $\delta\sigma = \sigma_{\mathrm{obs}} - [(M/L)\hat{\sigma}_{\mathrm{RMS}}^2 - k^2\,(M/L)\hat{V}^2]^{1/2}$. Here V_{sys} is the systemic velocity of the galaxy. We minimize these residuals in a χ^2 sense (i.e., squared, weighted with the formal uncertainties ΔV_{obs} and $\Delta\sigma_{\mathrm{obs}}$, and summed over all data points) to obtain the best-fitting values of M/L, k, and V_{sys}. The formal uncertainties on these quantities (i.e., those that reflect propagation of random uncertainties) follow from standard χ^2 theory. If the formal best fit for $|k|$ exceeds the maximum value $k_{\max}$ allowed for a physical model by equation (4), then we adopt the latter. In discussions of V_{obs} in the remainder of this paper it is to be understood that V_{sys} was always subtracted. The systemic velocities are of little interest by themselves (in the present context) and will not be discussed further.

The only parameter that is not generally constrained by the data is the inclination, which determines the axial ratio Q according to equation (6). One possibility is

TABLE 1
Intermediate-Redshift Galaxy Sample

ID (1)	Type (2)	$z_{\rm mod}$ (3)	$\rm PA_{maj}$ (4)	ϵ (5)	Q (6)	i (7)	FWHM (8)	$\sigma_{\rm eff}$ (9)	$\Delta\sigma_{\rm eff}$ (10)	M/L (11)	$\Delta M/L$ (12)	k (13)	$\Delta_- k$ (14)	$\Delta_+ k$ (15)
CL 3C295-568	S0/Sb	0.456	355	0.58	0.42	86.1	0.75	139	9	3.56	0.29	1.08*	0.01	0.00
CL 3C295-834	E	0.456	2	0.08	0.73	34.9	0.75	166	14	2.70	0.33	1.22	0.28	0.00
CL 3C295-868	S0	0.456	228	0.16	0.74	53.9	0.75	190	18	5.87	0.76	0.30*	0.36	0.36
CL 3C295-968	E	0.456	55	0.08	0.73	36.2	0.75	198	12	7.09	0.56	1.05	0.29	0.29
CL 3C295-2014	E/S0	0.456	327	0.19	0.73	58.5	0.75	231	18	5.93	0.63	1.72	0.56	0.04
CL 0016-438	E	0.546	358	0.08	0.73	34.2	0.91	216	13	3.78	0.35	0.42	0.44	0.44
CL 0016-461	E	0.546	312	0.33	0.62	72.7	0.79	262	23	6.51	0.56	0.50*	0.23	0.23
CL 0016-531	E	0.546	71	0.23	0.70	63.8	0.79	208	20	3.71	0.55	0.38*	0.47	0.47
CL 0016-611	E	0.546	143	0.14	0.75	49.1	0.91	163	17	2.59	0.46	1.30	0.46	0.00
CL 0016-612	E	0.546	319	0.13	0.75	46.9	0.91	265	37	4.19	0.42	0.55	0.65	0.65
CL 0016-650	E/S0	0.546	47	0.10	0.74	41.3	0.79	139	16	4.45	0.71	0.35*	0.45	0.45
CL 0016-659	E	0.546	90	0.22	0.71	62.0	0.79	249	26	5.74	0.82	0.08*	0.25	0.25
CL 0016-724	E	0.546	200	0.06	0.73	30.8	0.91	210	14	6.77	0.64	0.08	0.35	0.35
CL 0016-725	E	0.546	260	0.17	0.74	56.3	0.91	178	14	5.38	0.57	0.63*	0.20	0.20
CL 0016-745	E	0.546	174	0.12	0.75	45.6	0.91	114	13	1.89	0.29	1.38	0.30	0.00
CL 0016-2050	E	0.546	286	0.15	0.74	52.5	0.79	121	17	2.64	0.64	1.34*	0.09	0.00
CL 1601-270	S0/E	0.510	164	0.33	0.62	72.8	0.88	176	11	3.26	0.27	0.38*	0.16	0.16
CL 1601-292	E	0.539	55	0.19	0.73	58.1	0.71	169	11	2.77	0.23	1.37	0.21	0.00
CL 1601-524	E	0.539	11	0.13	0.75	47.1	0.71	210	15	5.65	0.42	0.83*	0.31	0.31
CL 1601-619	E	0.539	255	0.25	0.68	65.6	0.88	211	11	5.66	0.42	1.04*	0.24	0.24
CL 1601-753	E	0.539	75	0.16	0.74	54.5	0.71	248	11	6.19	0.25	0.03*	0.12	0.12
CL 1601-814	E	0.539	230	0.28	0.67	68.2	0.71	219	19	4.98	0.47	1.12*	0.27	0.11
CL 1601-2040	E	0.539	184	0.39	0.57	75.7	0.88	229	9	4.74	0.24	0.39*	0.07	0.07
CL 1601-2043	E	0.539	2	0.21	0.71	61.3	0.71	158	14	3.45	0.52	0.49	0.39	0.39
CL 1601-2060	E	0.539	336	0.25	0.69	65.1	0.71	218	33	5.91	0.56	1.17*	0.10	0.08

Note. — Column (1) lists the galaxy ID and column (2) the morphological type, both from Smail et al. (1997). Column (3) lists the redshift used for the modeling. For cluster members this is the redshift of the cluster from Dressler & Gunn (1992) and Dressler et al. (1999); for the field galaxy CL 1601-270 it is the observed redshift reported in vDvdM06. Column (4) lists the major axis position angle and column (5) the apparent ellipticity ($\epsilon = 1 - Q'$), both determined as described in Section 3.2. Column (6) lists the intrinsic axial ratio Q of our "standard" model, as defined by equation (9). Column (7) lists the corresponding inclination, calculated from equation (6). Column (8) lists the seeing FWHM of the spectroscopic observations in arcsec, determined by modeling the observed galaxy intensity profiles along the slit as described in Section 3.3. For the four galaxies that were observed with two different slit masks we list only the best value of the seeing. Columns (9) and (10) list the velocity dispersion for an aperture with the size of the effective radius, and its formal uncertainty. Columns (11)–(15) list the quantities inferred from our dynamical models with the standard axial ratio and inclination. Columns (11) and (12) list the best-fitting mass-to-light ratio (in solar B-band units) and its formal uncertainty. Columns (13)-(15) list the best-fitting rotational support and its formal uncertainties $k^{+\Delta_+ k}_{-\Delta_- k}$. If $\Delta_+ k = 0$ then this indicates that the best fit is obtained when k is set to the maximum value that guarantees positivity of σ_ϕ^2, as given by equation (4). An asterisk in column (13) indicates that the galaxy was included in the rotational support analysis presented in Section 4.

to assume that all galaxies are viewed edge-on, so that $i = 90^\circ$ and the intrinsic axial ratio is equal to the (observed) projected axial ratio: $Q = Q'$. Alternatively, one can assume that all galaxies have a small and fixed axial ratio, $Q = Q_{\rm min}$; we have taken $Q_{\rm min} = 0.4$ which is approximately the smallest intrinsic axial ratio found for early-type galaxies (Tremblay & Merritt 1995). The edge-on and $Q = Q_{\rm min}$ models are useful in that they produce, respectively, the roundest and flattest models possible, so that they bracket the range of available possibilities. However, since they both represent extremes, they are less useful for calculating the average properties of a large sample. For that purpose it is better to use models that are "correct" in an average statistical sense. To construct such models we used available knowledge on the projected axial ratio distribution $f(Q')$ of nearby early-type galaxies. Tremblay & Merritt (1995) inverted this distribution to obtain the distribution of intrinsic axial ratios $f(Q)$. They did so under various assumptions for the underlying geometry, and we use here their results for an oblate axisymmetric geometry. Given $f(Q)$, one can find[1] the distribution $f(Q|Q')$ that a galaxy of known projected axial ratio Q' has intrinsic axial ratio Q. In turn, this can be used to calculate the mean intrinsic axial ratio as function of projected axial ratio Q':

$$\langle Q\rangle(Q') \equiv \int Q f(Q|Q')\, dQ. \qquad (9)$$

In our models we set the intrinsic axial ratio Q of each galaxy to the value $\langle Q\rangle(Q')$ appropriate for its observed projected axial ratio Q'. We calculate the corresponding inclination from equation (6). We will refer to the values thus obtained as the "standard" axial ratio and inclination. Results discussed in the remainder of this paper are for these standard values. Our approach does not guarantee that we use the correct inclination for any individual galaxy. However, it does imply that our models

[1] We calculated $f(Q|Q')$ with a simple Monte-Carlo scheme in which for a very large number of hypothetical galaxies we perform the following steps: (a) draw a random three-dimensional viewing direction; (b) draw an intrinsic axial ratio Q from the distribution $f(Q)$; (c) calculate Q' from equation (6); (d) add the results to a joint frequency distribution of the quantities Q and Q'.

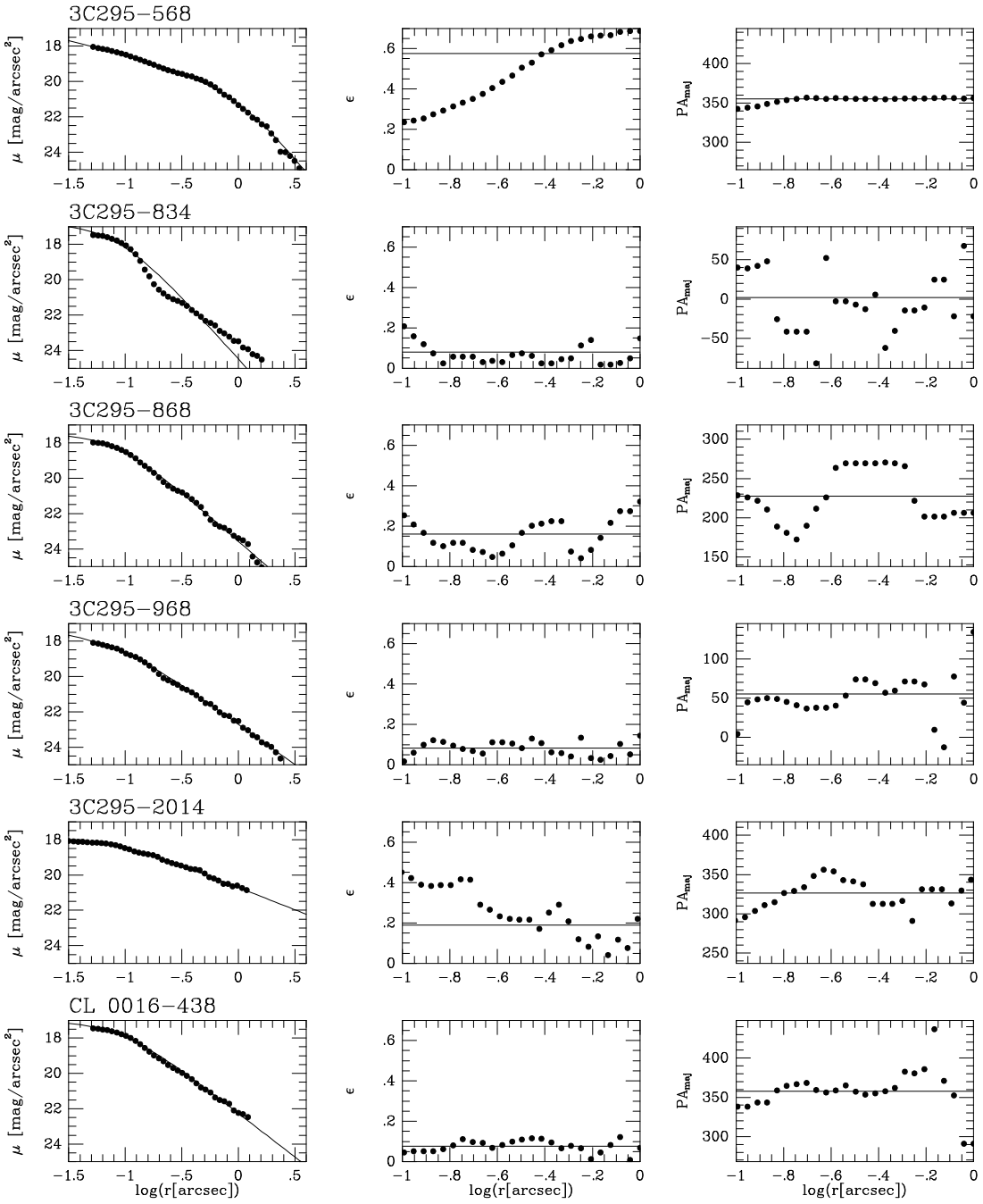

FIG. 1.— Elliptical isophote fit results for the sample galaxies as a function of semi-major axis length. Shown are from left to right: isophotal surface brightness, transformed to rest-frame B-band and corrected for $(1+z)^4$ cosmological surface brightness dimming; isophotal ellipticity; and major-axis position angle. The curves in the surface brightness panels show the predictions of the best-fit mass density models of the form given by equation (1). The horizontal lines in the ellipticity and position angle panels show the constant values used in the dynamical modeling (these are the weighted average values determined as described in Section 3.2).

have the correct average intrinsic axial ratios when averaged over a large sample. Where relevant, we address the dependence of the results on inclination by referring to results obtained with the edge-on models or $Q = Q_{\rm min}$ models.

3. RESULTS FOR INDIVIDUAL GALAXIES

3.1. *Sample*

For the modeling we used the sample of galaxies from vDvdM06. The galaxies reside in the clusters CL 3C295, CL 0016+1609, and CL 1601+4253, at redshifts $z =$ 0.456, 0.546, and 0.539, respectively (Dressler & Gunn 1992; Dressler et al. 1999). The clusters were selected based on their visibility at the time of the Keck observations, and because they are among the most S0 deficient clusters in the MORPHS sample (Dressler et al. 1997). The MORPHS sample itself was not selected according to strict criteria. The galaxy selection was largely constrained by the geometry of the Keck/LRIS masks, and by the fact that sample galaxies should be bright enough for spectroscopy. Priority was given to galaxies classified from HST images as E or E/S0 by Smail et al. (1999). The latest-type galaxy included in the sample was an

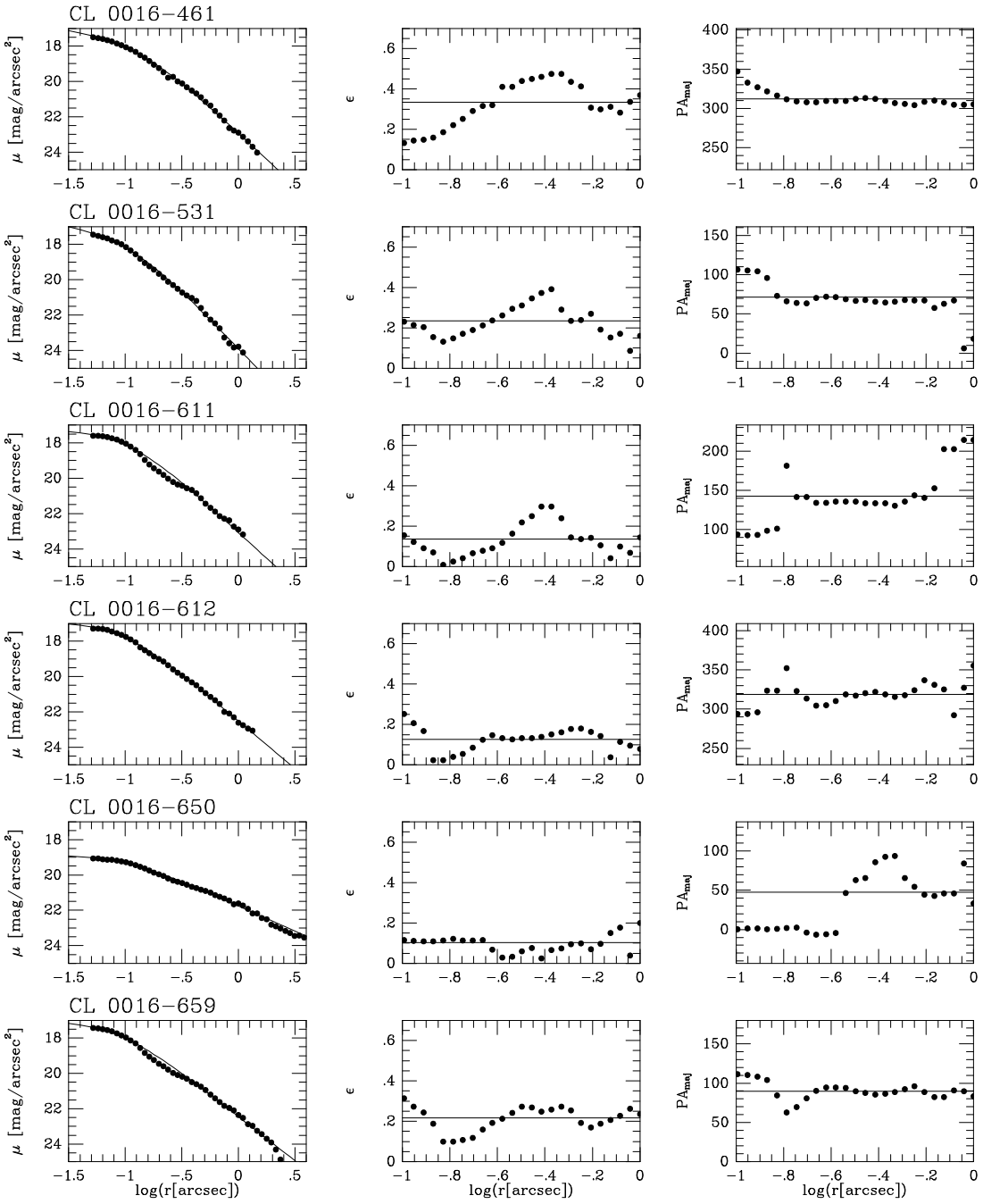

FIG. 1.— (continued)

S0/Sb galaxy. This galaxy 3C295-568 was included for the specific purpose to see if rotation could be measured reliably. For the present paper we excluded two galaxies from the sample of vDvdM06: 3C295-47 and CL1601-474. The former is a foreground field galaxy at $z = 0.131$. The latter has a disturbed morphology suggesting an ongoing merger, so that equilibrium models are likely to be of limited value. One other galaxy in the sample of vDvdM06 was found to be a field galaxy, namely CL 1601-270. This galaxy was retained because its redshift $z = 0.510$ is close to that of the other galaxies.

The galaxies in the final sample are listed in Table 1, including redshifts, visual classifications, and $\sigma_{\rm eff}$. The effective velocity dispersions are included for use in Paper II. They were calculated from the observed velocity dispersions measured from spectra that summed the central five pixels along each slit (presented in vDvdM). These measurements were transformed to an estimate of the dispersion inside an aperture of size $r_{\rm eff}$ using the formulae given in Jorgensen et al. (1995b). The values of $r_{\rm eff}$ and $I_{\rm eff}$ for the sample galaxies can be found in vDvdM06.

3.2. *Photometry*

To start the analysis we used the HST/WFPC2 images previously shown and discussed in vDvdM06. For the galaxies in the clusters CL3C295 and CL1601+42 there are only images in the F702W filter. For the galaxies in

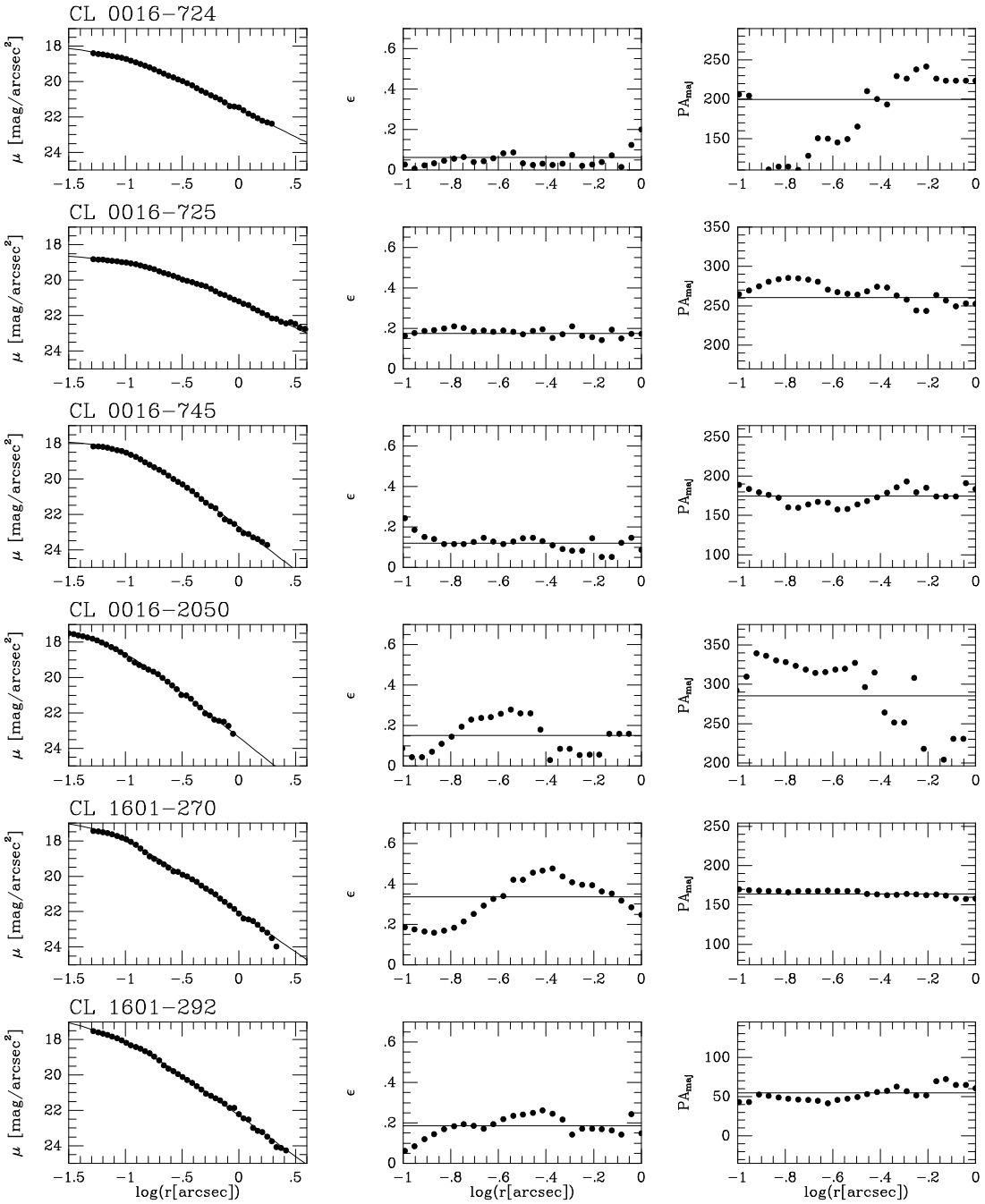

FIG. 1.— (continued)

the cluster CL0016+16 there are images in both F555W and F814W, but we only used the latter. The images were corrected for the blurring of the HST PSF using Lucy-Richardson deconvolution (Richardson 1972; Lucy 1974). The PSF used for the deconvolution was calculated with the TinyTim software package (Krist & Hook 2001). The deconvolved galaxy images were analyzed through isophotal ellipse fitting with the task `ELLIPSE` in the `IRAF` software package (Jedrzejewski 1987). This yields for each galaxy the major axis profile of surface brightness, ellipticity, and position angle. The results are shown in Figure 1. The profiles can generally be followed out to 1–5 arcsec from the galaxy center. The ellipticity and position angle are not shown in the figure inside 0.1 arcsec, where they are generally unreliable due to the residual effects of the HST PSF. They are also not shown outside of 1.0 arcsec, where they tend to become unreliable due to the low galaxy brightness relative to the sky brightness.

The models described in Section 2 are axisymmetric with constant axial ratio, and in projection have constant ellipticity $\epsilon = 1 - Q'$ and major axis position angle $\mathrm{PA_{maj}}$. To optimally choose these parameters for our models we calculated for each galaxy the average ellipticity and major axis position angle between 0.1 and 1 arcsec, weighted both with the flux and the annular area that each isophote represents. The results are listed in Table 1 and are also shown as horizontal lines in Figure 1.

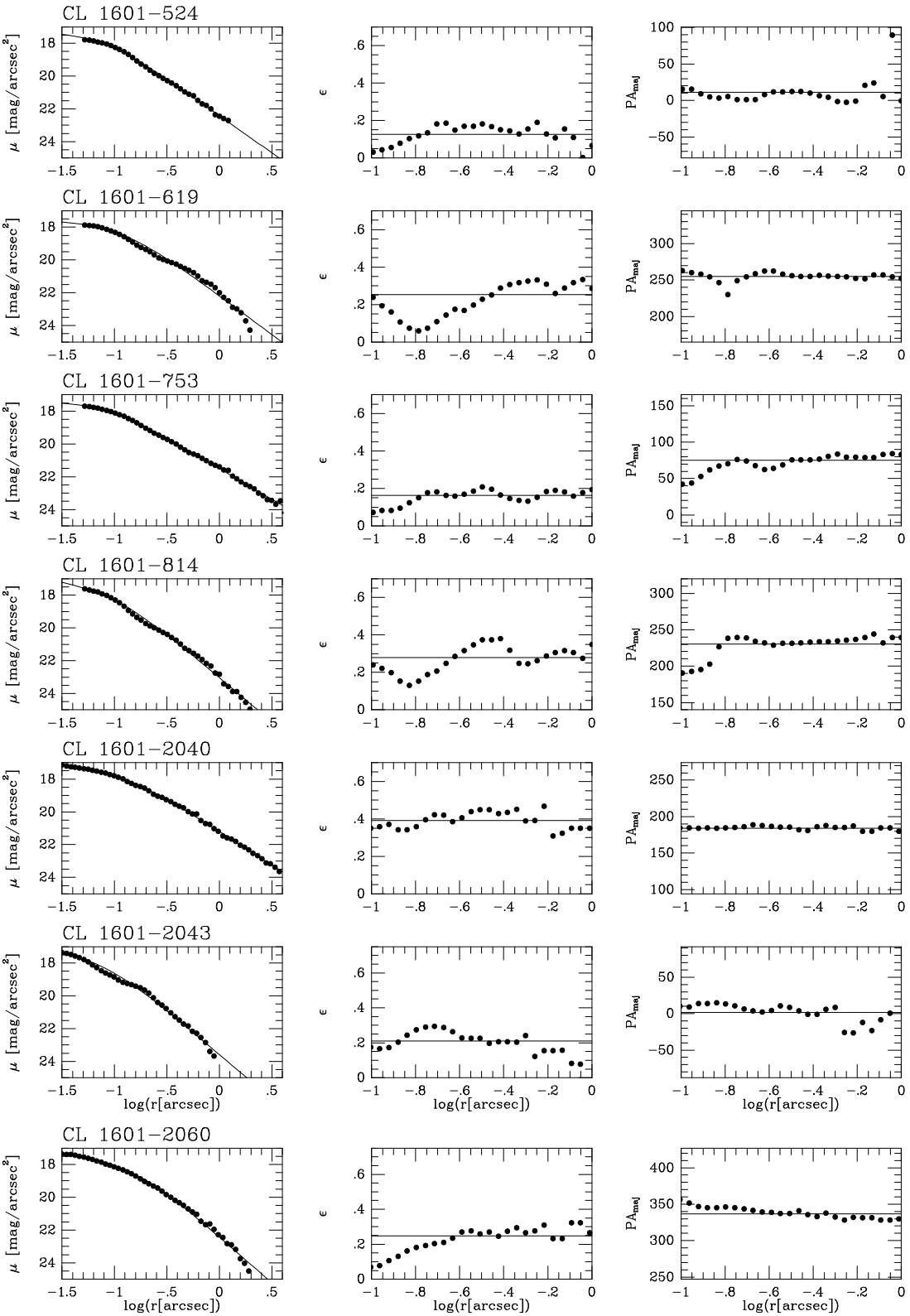

FIG. 1.— (continued)

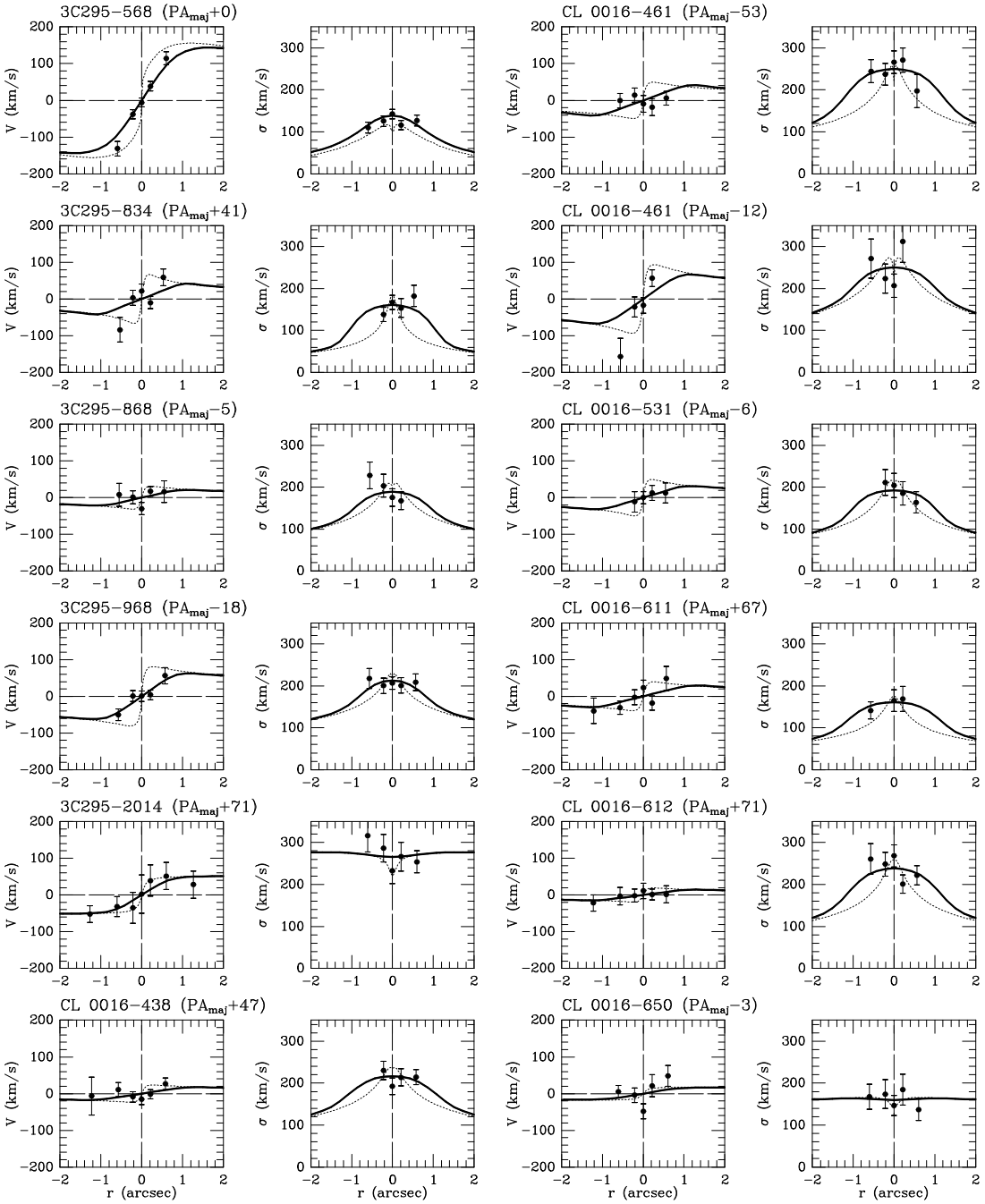

FIG. 2.— Kinematics of the sample galaxies. Each set of two adjacent panels show the rotation velocity V and the velocity dispersion σ along a given slit. The galaxy name is indicated in the label above the rotation velocity panel. The slit position angle is indicated in parentheses and is expressed as the sum of the major axis position angle given in Table 1 and an offset angle. The abscissa is given in arcsec. Data points are indicated with error bars. The heavy solid curves show the predictions of the best-fitting models with the standard inclination (see Table 1), taking into account the observational setup and spatial resolution. For comparison, the dashed curves show the model predictions as they would appear at infinite spatial resolution.

Clearly, the assumption of constant ellipticity and position angle with radius is better for some galaxies (e.g., CL1601-2040) than for others (e.g., CL0016-2050). However, even for galaxies with significant ellipticity variations or isophotal twists our approach still has the advantage that it properly takes into account some average measure of galaxy flattening.

The observed surface brightnesses in counts per second per pixel were transformed to magnitudes per square arcsecond using the known WFPC2 pixel sizes and filter zero-points from the WFPC2 Data Handbook (Baggett et al. 2002). The results were corrected for foreground Galactic extinction using the Schlegel et al. (1998) maps. The magnitudes in the filters used for the observations were then transformed to galaxy rest-frame B-band magnitudes using the relations given in vDvdM06. And finally, a $(1+z)^4$ correction for cosmological surface brightness dimming was applied.

For each galaxy we determined the parameters so that the projected luminosity density $\mu(x, y)$ of the model defined by equation (1) best fits the observed surface brightness profile. The fit was done using a Levenberg-

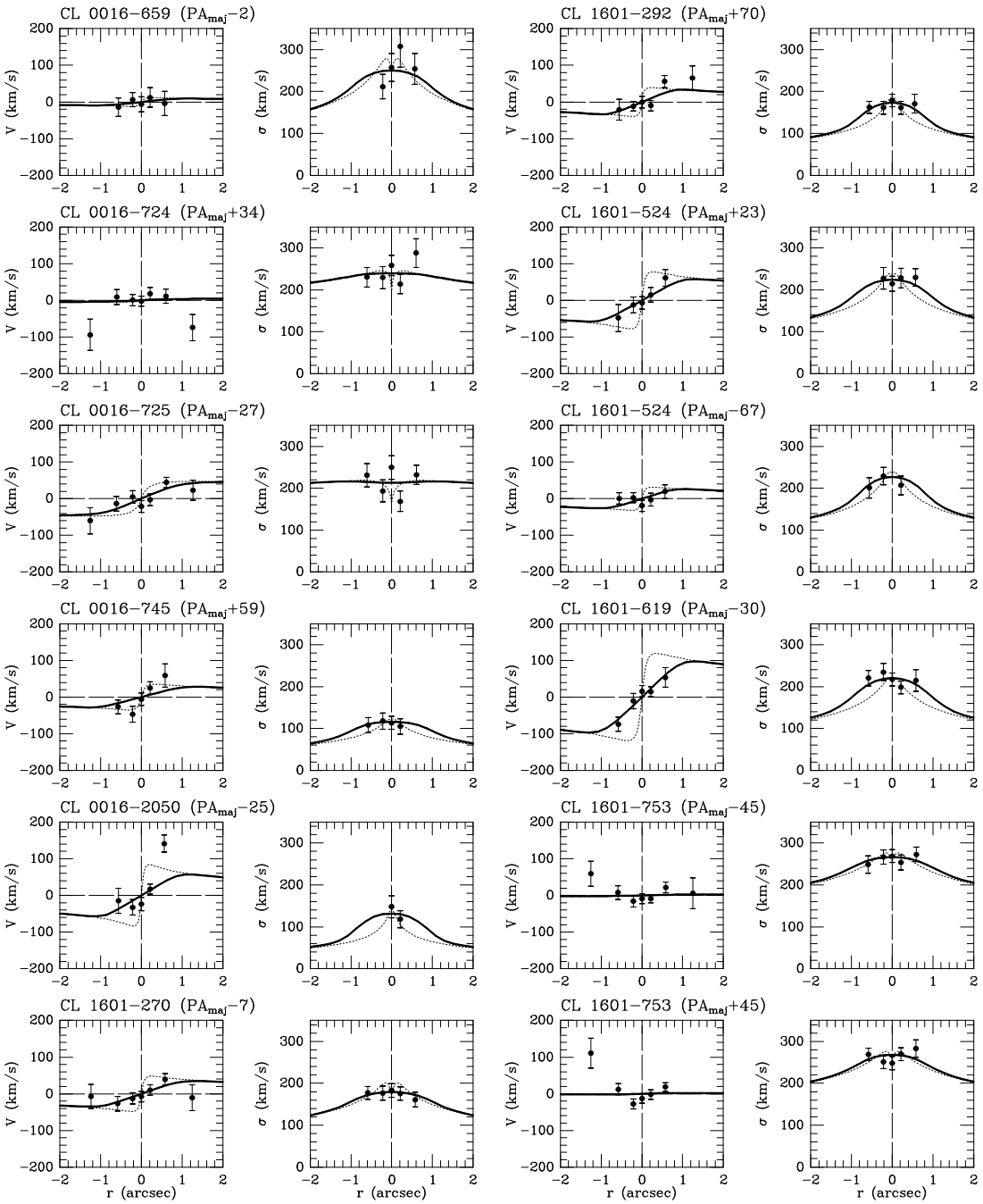

FIG. 2.— (continued)

Marquardt iteration scheme (Press et al. 1992). Data points within 2 arcsec from the galaxy center were included in the fit. The integrated brightness of the model in the central pixel was also included. The predictions of the best model fits are overplotted on the data in Figure 1. The predictions generally fit the observed surface brightness profiles reasonably well; the median residual over the entire sample is 0.09 mag/arcsec^2. The worst fit is obtained for CL 3C295-834, which clearly has more structure in its profile than can be accounted for by our model. The adopted inclination i and axial ratio Q for our standard model of each galaxy are listed in Table 1. For a given galaxy, the luminosity density j_0 is inversely proportional to Q because the total luminosity of the model, which is fixed by the observations, is proportional to $j_0 Q$. However, the inferred parameters b, α, and δ (see eq. [1]) and the fits shown in Figure 1 are all independent of the assumed i and Q.

The galaxy CL 3C295-2014 is the well-known AGN 3C295. There is the possibility that this galaxy contains a central non-thermal point source that could bias the analysis. However, the results for both the light profile of this galaxy and its M/L (see Figure 1 and Paper II) do not provide any evidence for deviations from the trends defined by the other galaxies in the sample. We therefore retained CL 3C295-2014 in our sample and did not treat it in any special way.

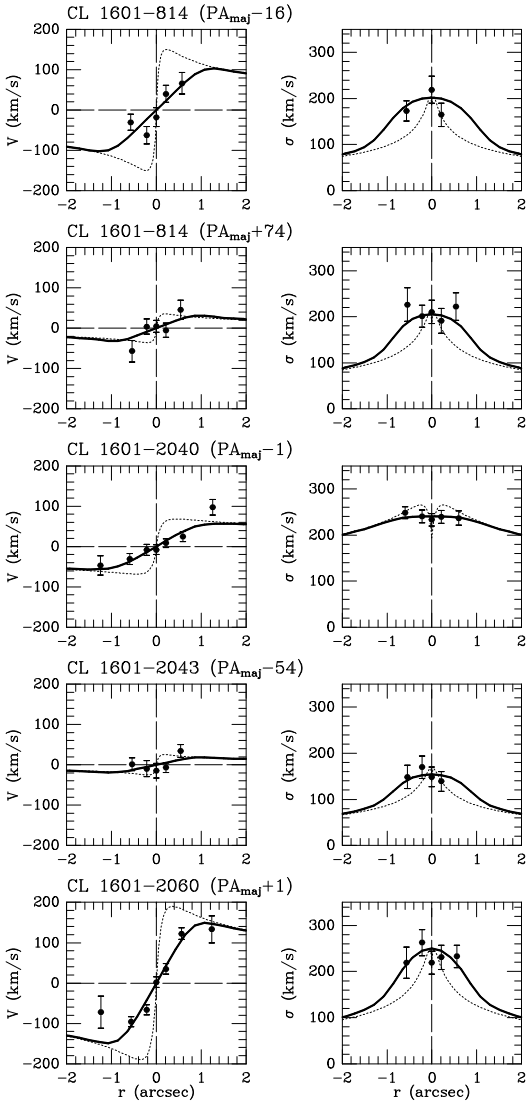

FIG. 2.— (continued)

3.3. *Kinematics*

For each galaxy we solved the Jeans equations to obtain predictions for the projected kinematics on the plane of the sky. To model the observational setup we used the known slit width $W = 1.1$ arcsec and pixel scale $P = 0.215$ arcsec/pixel. Binning along the slit that was applied to the data (see vDvdM06) was also taken into account. We assume that during the observations all slits were perfectly centered on their corresponding galaxy. This was probably true to within $\sim 0.2''$ accuracy. To determine the seeing for the observations with a given slit mask we ran models with different values of the FWHM S. We compared the observed and predicted intensity profiles along the slit for the galaxies observed with that mask, and adopted the value that gave the best agreement in a χ^2 sense. The inferred seeing FWHM values range from $0.71''$ to $0.91''$ (consistent with estimates obtained from inspection of stars observed during the same run) and are listed in Table 1. The position angle of each slit with respect to the galaxy major axis was determined by subtracting the value $\mathrm{PA_{maj}}$ in Table 1 from the known slit position angle on the sky. The values of the mass-to-light ratio M/L and rotational support k were determined to optimize the fit to the observed kinematics along the slit. For four galaxies (namely: CL0016-461, CL1601-524, CL1601-753, CL1601-814) data were available for more than one slit position angle (from observations with different slit masks). In those cases a single combination of M/L and k was fit simultaneously to the data for both slits.

Figure 2 shows the resolved kinematical profiles for all galaxies (obtained as described in Section 2.6 of vDvdM06), together with the best fits of the standard-inclination models. The fits are generally good, as confirmed by the χ^2 values. When summed over the entire sample, the mean velocity data points are fit with $\chi^2 = 145.8$ for 113 degrees of freedom. The velocity dispersion data points are fit with $\chi^2 = 81.1$ for 102 degrees of freedom. Models constructed with other assumptions for the inclination are both visually and statistically indistinguishable from those constructed for the standard inclinations. Comparison of edge-on models and models with $Q = Q_{\rm min}$ yields a difference in total χ^2, summed over the entire sample, of only $\Delta\chi^2 = 1.0$. This indicates that our kinematical data provide insufficient information to constrain the galaxy inclinations. Indeed, that would require high quality two-dimensional velocity fields (Cappellari et al. 2006).

For comparison, Figure 2 also shows the model predictions before convolution with the slit width, pixel size, and PSF. It is clear that this convolution has a major impact on the predictions, due to the fact that the spatial resolution of the observations is not much smaller than the galaxies themselves. In particular: (a) the observed rotation curves are always much shallower than the rotation curves that would be observed with infinite spatial resolution; and (b) the velocity dispersion profiles fall off less steeply with radius than they would when observed with infinite spatial resolution. Both effects are easily understood as the consequence of scattering of light from small radii (where the galaxy is brightest) to larger radii. Obviously, the resolved kinematics of distant galaxies can only be meaningfully interpreted if detailed dynamical models are combined with a proper accounting of the spatial resolution of the observations, as we have done here.

The kinematical data typically extend to between $0.2''$ and $1.2''$ from the galaxy center with a typical value of $\sim 0.7''$. At $z = 0.5$ this corresponds to 4.3 kpc. So our data extend about as far out as the data available for many nearby elliptical galaxies (e.g., van der Marel 1991; Emsellem et al. 2004). On the other hand, the sampling and resolution of the kinematical profiles in physical units are of course much worse. Nonetheless, for the mean velocities V it is clear that our spatially resolved measurements do provide important new insight on the internal structure of the galaxies as compared to a single integrated spectrum. The results for the S0/Sb galaxy 3C295-568 show that rotation can be reliable measured. While this is the most rapidly rotating galaxy in the sample (as expected, given its visual classification), most of the other galaxies also have statistically significant gradients in V along the slit. With the help of our models this provides constraints on the intrinsic rotation velocity. By contrast, for the velocity dispersions σ it is not clear that we are able to learn much more about the in-

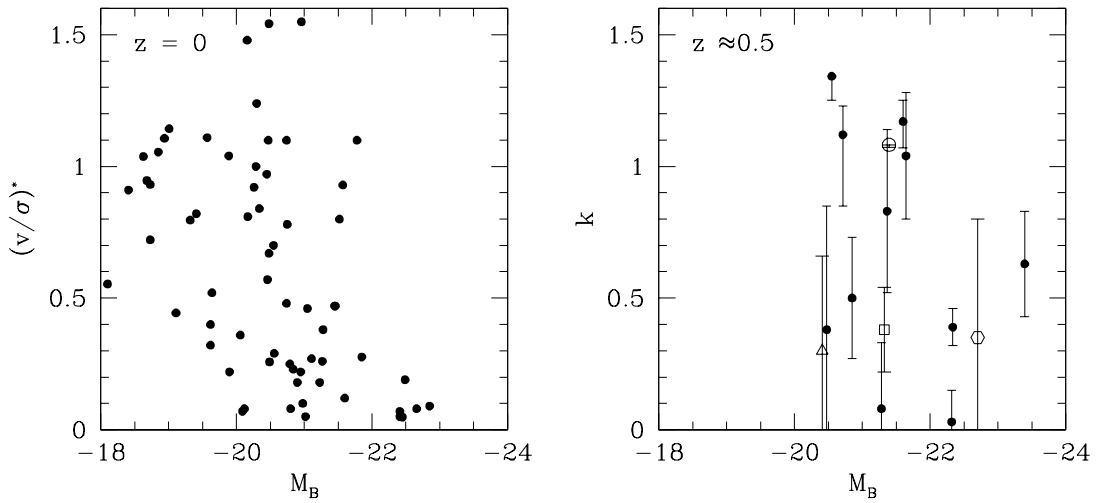

FIG. 3.— (a) $(v/\sigma)^*$ versus B-band absolute magnitude M_B for nearby elliptical galaxies. The data are from the compilations of Davies et al. (1983) and Bender, Burstein & Faber (1992). The M_B values from these papers were transformed to $H_0 = 71\,\mathrm{km\,s^{-1}\,Mpc^{-1}}$, for consistency with the value assumed here. (b) k versus M_B for the sample of intermediate redshift cluster galaxies. The values of M_B were corrected to $z = 0$ using the luminosity evolution calculated by vDvdM06, for comparison with the local sample. Symbol types indicate the visual galaxy classification from Smail et al. (1997): E (solid dot), E/S0 (hexagon), S0/E (square), S0 (triangle), or S0/Sa (open circle). Galaxies with apparent ellipticity $\epsilon < 0.10$ were excluded from both panels. For the intermediate redshift cluster sample, galaxies were included only if there is data along a slit within 45° from the major axis. In both panels, galaxies with $M_B \lesssim -20.4$ span a range of $(v/\sigma)^*$ or k values. However, most of these high-luminosity galaxies do not rotate fast enough to account for their flattening (i.e., they have $(v/\sigma)^* < 1$ or $k < 1$).

ternal structure than we would from a single integrated measurement. The model predictions in Figure 2 show that any gradients in σ over the central arcsec are expected to be small. To discriminate between different models one would need to be able to reliably measure these small gradients. In most galaxies our formal uncertainties on σ are not small enough to allow this. Of course, we do measure an accurate mass-to-light ratio, but that would have been possible also with only a single integrated σ measurement.

Table 1 lists the best-fitting values of k and M/L (in rest-frame B-band solar units) for the standard-inclination models, with their formal uncertainties. The sign of k is of little interest and indicates merely in which of two possible directions the galaxy is rotating around its symmetry axis. Adding 180° to the value of $\mathrm{PA_{maj}}$ yields a reversal of the sign of k. For convenience we have defined the values of $\mathrm{PA_{maj}}$ in Table 1 to be such that the best-fitting value of k is always positive. The M/L values of the galaxies are not addressed further here, since they are discussed and interpreted in detail in Paper II. Note that M/L depends on the assumed distance, and therefore on the assumed cosmological parameters Ω_m, Ω_Λ and H_0 (as listed in Section 1). The uncertainties in M/L introduced by distance uncertainties are not included in Table 1, but they are quantified in Paper II.

4. GALAXY ROTATION PROPERTIES

4.1. *Intermediate-Redshift Cluster Sample*

The model quantity k is a normalized measure of the rotation rate of a galaxy, with an oblate isotropic rotator model corresponding to $k = 1$. Inspection of Table 1 shows that the random uncertainties in k tend to be large when it is estimated from data along a slit that is far from the major axis, or for any galaxy that is nearly circular in projection on the sky. In these cases the value of k is also very sensitive to small systematic uncertainties in the measured major axis position angle or the ellipticity of the galaxy. For this reason we consider in the following only the 15 galaxies in the sample of intermediate redshift cluster galaxies for which a slit was placed within 45° of the major axis, and which have projected ellipticity $\epsilon > 0.10$. These galaxies are marked with an asterisk in column (13) of Table 1.

Figure 3b shows the inferred values of k as a function of the B-band absolute magnitude M_B. The latter was obtained from the total B-band luminosity, which was estimated as $L_B = 2\pi r_\mathrm{eff}^2 I_\mathrm{eff}$. For comparison to local samples, the luminosity was corrected to $z = 0$ using the luminosity evolution calculated by vDvdM06. The galaxies span a range of k values between 0 to about 1.3. The galaxies that were not visually classified as E galaxies are indicated with special symbols in the figure. The galaxies CL 0016-650 (E/S0), CL 1601-270 (S0/E) and CL 3C295-868 (S0) all have only modest rotation rates of $k = 0.3$–0.4, albeit with sizable uncertainties of similar magnitude. Either way, the rotation rates of these galaxies do not make them stand out among the ellipticals. By contrast, the galaxy CL 3C 295-568 (S0/Sb) has well-measured ($\Delta k \leq 0.01$) rapid rotation ($k \approx 1.08$). This galaxy also distinguishes itself among the sample galaxies by having the highest apparent flattening ($\epsilon = 0.58$).

4.2. *Comparison to Local Elliptical Galaxies*

The quantity that is most often measured for local galaxies to quantify rotational support is $(v/\sigma)^*$. This is defined as the ratio of the the observed (v/σ) and the value of (v/σ) expected for an oblate isotropic rotator model with the observed apparent flattening. This is almost identical to the model parameter k used here. The main difference is that $(v/\sigma)^*$ is defined in terms of projected global quantities (maximum rotation velocity and average velocity dispersion), whereas k is defined locally by equation (3). In principle this difference in definition could lead to small systematic differences between

k and $(v/\sigma)^*$, even when measured on the same galaxy. However, these differences are unlikely to exceed ~ 0.1. This is negligible compared to the typical uncertainties in our k measurements for the intermediate redshift cluster galaxies (see Figure 3b). In the following we therefore compare the quantity k directly to the quantity $(v/\sigma)^*$ available for local galaxies.

As local comparison sample we combined the literature compilations of $(v/\sigma)^*$ values for elliptical galaxies from Davies et al. (1983) and Bender, Burstein & Faber (1992). The resulting sample contains 80 galaxies. For consistency with our treatment of the sample of intermediate redshift cluster galaxies we excluded from the following discussion the 12 galaxies with $\epsilon < 0.10$.

Figure 3a shows $(v/\sigma)^*$ for the local ellipticals as a function of M_B. The local galaxies show a well-known trend between $(v/\sigma)^*$ and M_B. Low-luminosity ellipticals ($M_B \gtrsim -20.0$) have values of $(v/\sigma)^*$ that cluster near unity. This indicates that these galaxies are typically supported by rotation. High-luminosity ellipticals ($M_B \lesssim -20.0$) have values of $(v/\sigma)^*$ that range from zero to just above unity, but with most of the galaxies clustering near zero. This indicates that these galaxies are typically supported by velocity dispersion anisotropy (for a more detailed discussion of what $(v/\sigma)^*$ measurements imply for the velocity dispersion anisotropy of elliptical galaxies see Cappellari et al. 2005). The three galaxies in Figure 3a with $k \approx 1.5$ and M_B between -20.0 and -21.0 are NGC 584, 2974, and 3640. These are probably not normal ellipticals. NGC 584 is actually classified in the RSA catalog (Sandage & Tammann 1981) as an S0 galaxy, although it is an E4 in the RC3. NGC 2974 is also an E4 galaxy, but it has all the hallmarks of being a misclassified S0 galaxy (Cinzano & van der Marel 1994). And NGC 3640 has considerable fine-structure that suggests it is a recent merger remnant (Prugniel et al. 1988).

The galaxies in the sample of intermediate redshift cluster galaxies are all brighter than $M_B \approx -20.0$. The fact that they span a wide range of k values is therefore consistent with the behavior seen in the local sample. Moreover, the four brightest galaxies ($M_B < -22.0$) all appear to have insufficient rotation to account for their flattening, consistent with the situation for the elliptical galaxies in the nearby universe. However, the details of the distribution of rotational support are somewhat different between the local and distant samples. Figure 4 compares a histogram of the k values for the intermediate redshift cluster galaxies to a histogram of the $(v/\sigma)^*$ values of local galaxies. For the intermediate redshift cluster galaxies we included only the 11 galaxies classified as ellipticals, for consistency with the local sample. For the local galaxies we included only galaxies with $M_B < -20.4$. With this selection, both histograms probe similar absolute magnitude ranges (for the local sample M_B has an average of -21.2 with a dispersion of 0.7 and for the distant sample it has an average of -21.5 with a dispersion of 0.9).

The histograms in Figure 4 show that in a relative sense there is a higher number of rapidly rotating galaxies in the distant sample than in the local sample. The average $\langle k \rangle$ for the distant galaxies is 0.68 ± 0.13, whereas the average $\langle (v/\sigma)^* \rangle$ for the local galaxies is 0.47 ± 0.07. In the distant sample 36% of the galaxies have $k > 0.9$, whereas

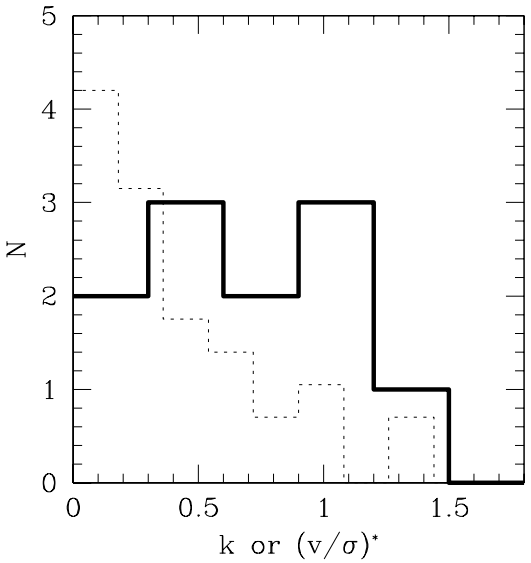

FIG. 4.— Comparison of a histogram of the k values for the intermediate redshift cluster galaxies (heavy line) to a histogram of the $(v/\sigma)^*$ values of local galaxies (dotted line). For the intermediate redshift cluster galaxies we included only the 11 galaxies with reliable k determinations that were classified as ellipticals, for consistency with the local sample. For the local galaxies we included only galaxies with $M_B < -20.4$, so that both histograms probe similar absolute magnitude ranges. The histograms show that in a relative sense there is a higher number of rapidly rotating galaxies in the distant sample than in the local sample.

in the local sample only 19% have $(v/\sigma)^* > 0.9$. This estimate of the percentage difference at high rotation rates is actually conservative for two reasons. First, the percentage of the local sample with $(v/\sigma)^* > 0.9$ would drop by 5% if we excluded the two potential S0 galaxies NGC 584 and 2974. And second, values of $(v/\sigma)^*$ are defined as the rotational support for an edge-on model. In contrast, our standard two-integral models are somewhat inclined. If instead we had used the values of k inferred from edge-on models for the intermediate redshift clusters, then all k values would have gone up by $\sim 7\%$. The discrepancy between the histograms in Figure 4 would then have been even larger. In view of the statistics and these additional considerations, we conclude that the difference between the rotation properties of the galaxies in our $z \approx 0.5$ cluster sample and those of our local comparison sample are significant. In the following subsections we discuss possible explanations for this difference.

4.3. *S0 Misclassification*

One plausible explanation for the relatively high fraction of rapidly rotating galaxies at $z \approx 0.5$ is that the fraction of misclassified S0 galaxies among visually classified elliptical galaxies is larger in intermediate-redshift clusters than it is locally. This has in fact been suggested (e.g., Fabricant et al. 2000) as a possible explanation for the low fraction of S0 galaxies found in intermediate-redshift clusters (Dressler et al. 1997). The bulges of S0 and spiral galaxies typically have rotation rates consistent with oblate isotropic rotator models (Davies et al. 1983). Any contamination from disk light will further increase the observed rotation. Therefore, one would normally expect to find S0 galaxies at values of k or $(v/\sigma)^*$ near or above unity.

Based on the statistics for the local comparison sam-

ple one would have expected $0.19 \times 11 = 2.1$ galaxies in the distant galaxy histogram in Figure 4 with $k > 0.9$. Instead, 4 out of 11 are observed to have such high rotation rates. We excluded 4 galaxies with $\epsilon < 0.10$ from the histogram. These are unlikely to be S0 galaxies, since the solid angle under which galaxies are viewed pole-on is small. Hence, we estimate that 13% (namely, $(4-2.1)/(11+4)$) of the elliptical galaxies in these intermediate redshift clusters might be misclassified S0 galaxies. The average of the morphological percentages reported by Dressler et al. (1997) for the three clusters studied here are E:S0:Spirals = 47:16:37. Upon correction for the suggested misclassification of S0s as ellipticals we obtain instead 41:22:37. Although correcting for misclassifications increases the S0 fraction of these clusters, it remains much smaller than the $\sim 60\%$ found in local clusters (Dressler 1980). So there appears to be a strong evolution in the real fraction of S0 galaxies in clusters. Our data do not suggest that this can be attributed to misclassification, although it should be kept in mind that the S0 fraction in intermediate redshift clusters might be higher than what we just estimated. Not all S0 galaxies would necessarily be recognized from their kinematics alone.

Our results with respect to potential S0 misclassification probably depend on the sample selection. The three clusters in our sample were selected based on their low fractions of visually-classified S0 galaxies (see Section 3.1). On the one hand, this makes these clusters good test cases: there are many visually-classified elliptical galaxies that could potentially be misclassified S0 galaxies. On the other hand, if these clusters are truly poor in S0 galaxies, then they are not good test cases: in that case there simply aren't many S0 galaxies that one could potentially misclassify. Therefore, the results presented here may not generalize to other clusters at similar redshift that have higher S0 fractions based on visual classification.

4.4. *Redshift Evolution of Galaxy Rotational Support through Mergers*

An alternative interpretation for the difference between the histograms in Figure 4 is to assume that there is a true redshift evolution in the internal dynamics of elliptical galaxies. Since elliptical galaxies are collisionless systems, mergers are required to significantly change their rotation rate. There are different types of mergers and these can affect the evolution of the observed rotation rate in different ways. We will discuss the relevant types in turn. Independent of the type of merger, we are only concerned here with mergers that happen between $z \approx 0.5$ and $z = 0$, i.e., in the last 5 Gyr.

Mergers between spiral galaxies form remnants that resemble elliptical galaxies (e.g., Barnes 1988). The progenitors of such mergers are not included in samples of elliptical galaxies at intermediate redshift. However, the remnants of such mergers are included in local samples of elliptical galaxies. Such mergers therefore contribute to the so-called "progenitor bias" (e.g., van Dokkum & Franx 2001). Dissipationless and dissipational simulations show that the remnants of disk-disk mergers have properties that are similar to local low-luminosity ellipticals, which tend to be disky and flattened by rotation (Naab & Burkert 2003; Naab et al. 2006b). In contrast, disk-disk mergers do not seem a plausible formation mechanism for the most luminous ellipticals, since only equal-mass mergers with special initial orientations can produce purely boxy anisotropic merger remnants. So if it were possible to remove from the local sample in Figure 4 the ellipticals that formed from disk-disk mergers since $z \approx 0.5$, then this would probably *decrease* the relative proportion of rapidly-rotating ellipticals. Therefore, progenitor bias due to disk-disk mergers cannot explain the evolution seen in Figure 4. In fact, the progenitor bias is such that the observed evolution is probably only a lower limit to the true evolution.

The situation is different for mergers between elliptical galaxies. The progenitors of such mergers are included in samples of elliptical galaxies at intermediate redshift. Therefore, such mergers introduce no progenitor bias (provided that luminosity-dependent sample selection effects are properly understood). Simulations show that the remnants of mergers between early-type galaxies have properties that are similar to luminous ellipticals in the local universe (Naab et al. 2006a). In particular, the rotation rate of the remnants is generally low, even when the progenitors were flattened by rotation. Because elliptical galaxies have little gas, there is no formation of a gas disk in the merger remnant that can form stars and boost the observed rotation rate (in contrast to the situation for disk-disk mergers; Naab et al. 2006b). Therefore, dissipationless ("dry") mergers between elliptical galaxies can produce evolution in the elliptical galaxy population towards lower rotation rates. This would be consistent with the evolution seen in Figure 4.

The importance of mergers for the evolution seen in Figure 4 depends on the number of mergers of the relevant types in the last 5 Gyr. There is observational evidence that merging is indeed happening at an important rate in this time interval. Most studies originally lumped various types of interactions and mergers together (e.g., Le Fèvre et al. 2000; Patton et al. 2002; Conselice et al. 2003; Lin et al. 2004; Bundy et al. 2004). However, some recent studies have aimed to separate mergers of different types to specifically demonstrate the importance of dry merging (e.g., van Dokkum 2005). Bell et al. (2006) used data for galaxies in the GEMS survey to estimate that present-day spheroidal galaxies with $M_V < -20.5$ have on average undergone between 0.5 and 2 dry mergers since $z \approx 0.7$. Semi-analytical models of hierarchical structure formation predict that in the mass-range of interest to the present study, disk-disk mergers are about as common as dry mergers (Naab et al. 2006a). Both types of mergers are therefore likely to have been numerous enough in the last 5 Gyr to have affected a significant fraction of elliptical galaxies in the luminosity range covered by our sample.

Most observational work of the merger rate as a function of redshift has studied field galaxies. While these studies have shown that mergers are important, this does not necessarily imply that our results have been affected by them. This is because the frequency of merging depends on environment. Our local comparison sample of elliptical galaxy rotation rates (see Section 4.2) is composed mostly of galaxies in the field and in low-density cluster environments such as Virgo. This range of environments is probably not too dissimilar from that probed by field galaxy surveys out to significant redshifts. This

assumption implies that disk-disk mergers in the last 5 Gyr have probably been numerous enough among our local comparison sample to have affected the results in Figure 4 through the progenitor bias previously eluded to.

Whether dry mergers have been numerous enough to decrease the rotation rates of the elliptical galaxies in our intermediate-redshift sample is a different issue. This is because those galaxies reside in dense clusters. The traditional belief has been that galaxy interactions in clusters are different from those in the field due to the large relative velocities between galaxies. Galaxy transformations can then occur due to the cumulative effect of frequent high speed galaxy encounters ("galaxy harassment"; Moore et al. 1996). However, calculations of merger rates (based mostly on somewhat idealized simulations without a cosmological context; e.g., Makino & Hut 1997) show that true mergers may be rare (except for accretion events onto the brightest cluster galaxy). However, recent observations have challenged this paradigm. In particular, van Dokkum et al. (1999) and Tran et al. (2005) found direct observational evidence for ongoing mergers in the cluster MS 1054-03 at $z = 0.83$. The true abundance of dry mergers in clusters therefore remains unclear. However, it does appear possible that dry mergers in clusters may have caused a decline in the rotation rate of elliptical galaxies over the last 5 Gyr.

4.5. *Environmental Dependence and Cosmic Variance*

A final possible explanation for the difference between the rotation rates of our sample galaxies at $z \approx 0.5$ and those of the local comparison sample of Section 4.2 is that the average rotation rate of elliptical galaxies may not be the same at different locations in the Universe. There could be a dependence on environment or there could be significant statistical fluctuations between widely separated locations (cosmic variance). Our intermediate-redshift sample consists of galaxies in dense clusters. In contrast, our local comparison sample contains an inhomogeneous mixture of galaxies in cluster, group and field environments. A dependence on environment would therefore be particularly relevant for the comparison. However, observations in the local universe have provided no evidence that such a dependence exists. The $(v/\sigma)^*$ distributions of the rare elliptical galaxies in very low-density environments are quite similar to those for local samples biased towards high-density environments (Hau & Forbes 2006). Current cosmological models do not have the resolution or detailed physics that would be needed to make confident predictions for the size of either an environmental dependence or cosmic variance in the elliptical galaxy rotation rate. A good way to address this will therefore be to study larger samples of intermediate-redshift galaxies in a wider range of locations and environments.

5. SUMMARY AND DISCUSSION

We have presented detailed dynamical models for the spatially resolved kinematics of 25 galaxies in the intermediate-redshift ($z \approx 0.5$) clusters CL3C295, CL0016+16 and CL1601+42. The sample galaxies were selected to be bright enough for spectroscopy, and visually classified from HST images as early type (and in most cases elliptical) galaxies. The spectroscopic data were obtained with LRIS on Keck as described in vDvdM06, with a $1.1''$ wide slit in seeing of $0.71''$ to $0.91''$ FWHM. The data sample a region that extends typically to $\sim 0.7''$ from the galaxy center (~ 4.3 kpc) sampled at $0.215''$ per pixel.

To model the data we adopted an oblate axisymmetric luminosity density of fixed axial ratio for each galaxy that fits the surface brightness profile inferred from HST imaging. The inclination of the models was chosen to provide the most likely intrinsic axial ratios in a statistical sense. Edge-on models and highly-flattened models were also explored, but the results do not depend strongly on the assumed inclination. For each galaxy we solved the Jeans equations of hydrostatic equilibrium under the assumption that the distribution function has the two-integral form $f = f(E, L_z)$. The resulting model predictions were projected along the line of sight and convolved with the observational seeing, slit width, and binning along the slit. Accounting for the observational characteristics is crucial for a proper interpretation of resolved kinematical data obtained at these redshifts, and in particular the rotation curves. When this is done, the model predictions overall provide good fits to the kinematical data.

Comparison of models and observations yields for each galaxy a quantity k that is a normalized measure of the rotation rate of the galaxy. This quantity is similar to the quantity $(v/\sigma)^*$ that is often used to measure the rotation rate of nearby galaxies (where $k = (v/\sigma)^* = 1$ for an oblate isotropic rotator model). To quantify the rotational properties of the sample galaxies we studied how k behaves as a function of galaxy magnitude M_B. We compared this to the known correlations between $(v/\sigma)^*$ and M_B for elliptical galaxies in the local Universe. We find that the intermediate-redshift ellipticals span a large range in k from about 0 to 1.3. This is not dissimilar from what is seen locally for elliptical galaxies of similar luminosity. The four brightest galaxies in the sample, which will have $M_B < -22$ even when evolved forward in time to $z = 0$, all rotate too slowly to account for their flattening. This is consistent with what is seen in the local Universe for galaxies of the same luminosity. Nonetheless, in a relative sense there is a higher number of rapidly rotating galaxies in the intermediate-redshift sample than in the local Universe (when comparing galaxies of similar present-day luminosity).

The general similarity of the rotation rates of the sample galaxies to those of local ellipticals suggests that the intermediate-redshift galaxies have in large majority been correctly classified visually as early-type galaxies. Nonetheless, a possible explanation for the higher rotation rates of the galaxies at $z \approx 0.5$ is that the fraction of misclassified S0 galaxies among visually classified elliptical galaxies is larger in intermediate-redshift clusters than it is locally. If this is indeed the cause of the observed effect, then the S0 galaxy fraction in the target clusters may have been underestimated by $\sim 6\%$. Even if this were the case, a strong evolution in the S0 fraction of clusters continues to be implied between the local Universe (where the fraction is $\sim 60\%$) and $z \approx 0.5$ (where for the three clusters studied here the fraction is only $\sim 22\%$, even after the listed upward correction). A popular explanation for this evolution is that many local S0 galaxies may have recently transformed from

star-forming spiral galaxies. However, this explanation is not without problems. Substantial differences would be expected between the mean M/L and color of S0s and ellipticals, which are not observed (van Dokkum & Franx 2001). The contribution of misclassification to the observed evolution should therefore remain a topic of investigation, in particular since not all misclassified S0 galaxies would necessarily be recognized from their kinematics alone.

Mergers can be another reason why there is a decrease in the observed average rotation rate between $z \approx 0.5$ and the present. Dissipationless (dry) mergers between early-type galaxies can decrease the average rotation rate of the population, which is qualitatively consistent with the direction of the observed trend. However, it is unclear whether such mergers are numerous enough in the high-velocity-dispersion environment of dense clusters to reproduce the observed size of the trend. By contrast, disk-disk mergers contribute to the comparison of our sample to local galaxies only through the so-called "progenitor bias". Elliptical galaxies in the local sample that formed from such mergers in the last 5 Gyr would not be represented in the intermediate-redshift sample, which is composed of visually-classified elliptical galaxies. This cannot explain the observed trends though, because it increases rather than decreases the relative number of rapidly rotating galaxies in the local Universe. However, such mergers are numerous enough that their progenitor bias must be taken into account in any quantitative attempts to explain the observed trends.

With large aperture telescopes and multi-slit capabilities it is now possible to study the resolved kinematics of large samples of galaxies at intermediate redshifts. As we have shown here, detailed dynamical modeling of such data has the potential to provide new insights into the evolution of galaxies. This provides important advantages over studies that are based solely on global quantities. For example, changes in the rotation rates of galaxies as a function of redshift can probe their merger history. It therefore seems useful to perform more studies like the one presented here in the near future, to explore wider ranges of redshifts, environments, and galaxy types. Such studies would also explicitly constrain the contribution to the observed differences in rotation rates between local elliptical galaxies and those at intermediate redshifts due to potential environmental dependencies and cosmic variance.

The models that we have constructed here also yield the mass-to-light ratios M/L for all the sample galaxies. These are used in Paper II to study the M/L evolution of elliptical galaxies as a function of redshift, which in turn constrains the formation ages of elliptical galaxies. This complements and tests analyses based on Fundamental Plane evolution, such as those presented in vDvdM06.

We thank Thorsten Naab for useful discussions. Part of this research was carried out at the Kavli Institute for Theoretical Physics in Santa Barbara, supported in part by the National Science Foundation under Grant No. PHY99-07949.

REFERENCES

Baggett, S., et al. 2002, in HST WFPC2 Data Handbook, v. 4.0, ed. B. Mobasher (Baltimore: STScI)
Barnes, J. E. 1988, ApJ, 331, 699
Bell, E. F. 2006, ApJ, 640, 241
Bender, R., Burstein, D., & Faber, S. M. 1992, ApJ, 399, 462
Binney, J. J., Davies, R. L., & Illingworth, G. D. 1990, ApJ, 361, 78
Binney, J. J., & Merrifield, M. 1998, Galactic Astronomy (Princeton: Princeton University Press)
Binney, J., & Tremaine, S. 1987, Galactic Dynamics (Princeton: Princeton University Press)
Bundy, K., Fukugita, M., Ellis, R. S., Kodama, T., & Conselice, C. J. 2004, ApJ, 601, L123
Cappellari, M., et al. 2005, in "Nearly Normal Galaxies in a LCDM Universe", http://astro.ucsc.edu/∼nng/posters.html [astro-ph/0509470]
Cappellari, M., et al. 2006, MNRAS, 366, 1126
Cinzano, P., & van der Marel, R. P. 1994, 270, 325
Conselice, C. J., Bershady, M. A., Dickinson, M., & Papovich, C. 2003, AJ, 126, 1183
Corsini, E. M., et al. 1999, A&A, 342, 671
Davies, R. L., Efstathiou, G., Fall, S. M., Illingworth, G., Schechter, P. L. 1983, ApJ, 266, 41
De Lucia, G., et al. 2004, ApJ, 610, L77
Dressler, A. 1980, ApJ, 236, 351
Dressler, A., & Gunn, J. E. 1992, ApJS, 78, 1
Dressler, A., et al. 1997, ApJ, 490, 577
Dressler, A., Smail, I., Poggianti, B. M., Butcher, H., Couch, W. J., Ellis, R. S., Oemler, A. Jr. 1999, ApJS, 122, 51
Emsellem, E., et al. 2004, MNRAS, 352, 721
Fabricant, D., Franx, M., & van Dokkum, P. 2000, ApJ, 539, 577
Freedman, W. L., et al. 2001, ApJ, 553, 47
Gebhardt, K., et al. 2003, ApJ, 583, 92
Hau, G. K. T., & Forbes, D. A. 2006, MNRAS, 371, 633
Jedrzejewski, R. I. 1987, MNRAS, 226, 747
Kelson, D. D., Illingworth, G. D., van Dokkum, P. G., & Franx, M. 2000, ApJ, 531, 159
Koopmans, L. V. E., Treu, T., Bolton, A. S., Burles, S., & Moustakas, L. A. 2006, ApJ, 649, 599
Krist, J., & Hook, R. 2001, The Tiny Tim User's Guide, (Baltimore: STScI)
Kronawitter, A., Saglia, R. P., Gerhard, O., & Bender, R. 2000, A&AS, 144, 53
Le Fèvre, O, et al. 2000, MNRAS, 311, 565
Lin, L. et al. 2004, ApJ, 617, L9
Lucy, L. B. 1974, AJ, 79, 745
Magorrian, J., et al. 1998, AJ, 115, 2285
Makino, J., & Hut, P. 1997, ApJ, 481, 83
Mei, S., et al. 2006, ApJ, 644, 759
Moore, B., Katz, N., Lake, G., Dressler, A., & Oemler, A., Jr. 1996, Nature, 379, 613
Naab, T., & Burkert, A. 2003, ApJ, 597, 893
Naab, T., Jesseit, R., & Burkert, A. 2006b, MNRAS, 372, 839
Naab, T., Khochfar, S., & Burkert, A. 2006a, ApJ, L81
Patton, D. R., et al. 2002, ApJ, 565, 208
Press, W. H., Teukolsky, S. A., Vetterling, W. T., & Flannery, B. P. 1992, Numerical Recipes (Cambridge: Cambridge University Press)
Prugniel., P., Nieto, J.-L., Davoust, E., & Bender, R. 1988, A&, 204, 61
Richardson, W. H. 1972, J. Opt. Soc. A., 62, 52
Sandage, A., & Tammann, G. A. 1981, A Revised Shapley-Ames Catalog of Bright Galaxies (Washington, D.C: Carnegie Institution of Washington) (RSA)
Schlegel, D. J., Finkbeiner, D. P., & Davis, M. 1998, ApJ, 500, 525
Smail, I., Dressler, A., Couch, W. J., Ellis, R. S., Oemler, A., Jr., Butcher, H., Sharples, R. M. 1997, ApJS, 110, 213
Spergel, D. N., et al. 2003, ApJS, 148, 175
Tran, K.-V. H., van Dokkum, P., Franx, M., Illingworth, G. D., Kelson, D. D., Förster Schreiber, N. 2005, ApJ, 627, L25
Tremblay, B., & Merritt, D. 1995, AJ, 110, 1039
Treu, T., & Koopmans, L. V. E. 2004, ApJ, 611, 739
van der Marel, R. P. 1991, MNRAS, 248, 515
van der Marel, R. P., Evans, N. W., Rix, H.-W., White, S. D. M., & de Zeeuw, P. T. 1994b, MNRAS, 271, 99
van der Marel, R. P., Cretton, N., de Zeeuw, P. T., & Rix, Hans-Walter 1998, ApJ, 493, 613
van der Marel, R. P. & van Dokkum, P. G. 2006, ApJ, submitted (Paper II)
van Dokkum, P. G., Franx, M., Fabricant, D., Kelson, D. D., & Illingworth, G. D. 1999, ApJ, 520, L95
van Dokkum, P. G., & Franx, M. 2001, ApJ, 553, 90
van Dokkum, P. G. 2005, AJ, 130, 2647

van Dokkum, P. G., & van der Marel, R. P. 2006, ApJ, in press (vDvdM06) [astro-ph/0609587]